THE JOURNAL OF PHYSICAL CHEMISTRY Letters

pubs.acs.org/JPCL Letter

Controlling Thermal Conductivity in Mesoporous Silica Films Using Pore Size and Nanoscale Architecture

Yan Yan, Man Li, Sophia King, Tiphaine Galy, Michal Marszewski, Joon Sang Kang, Laurent Pilon, Yongjie Hu, and Sarah H. Tolbert*

Cite This: J. Phys. Chem. Lett. 2020, 11, 3731−3737 Read Online

ACCESS | Metrics & More | Article Recommendations | Supporting Information

ABSTRACT: This work investigates the effect of wall thickness on the thermal conductivity of mesoporous silica materials made from different precursors. Sol−gel- and nanoparticle-based mesoporous silica films were synthesized by evaporation-induced self-assembly using either tetraethyl orthosilicate or premade silica nanoparticles. Since wall thickness and pore size are correlated, a variety of polymer templates were used to achieve pore sizes ranging from 3−23 nm for sol−gel-based materials and 10−70 nm for nanoparticle-based materials. We found that the type of nanoscale precursor determines how changing the wall thickness affects the resulting thermal conductivity. The data indicate that the thermal conductivity of sol−gel-derived porous silica decreased with decreasing wall thickness, while for nanoparticle-based mesoporous silica, the wall thickness had little effect on the thermal conductivity. This work expands our understanding of heat transfer at the nanoscale and opens opportunities for tailoring the thermal conductivity of nanostructured materials by means other than porosity and composition.

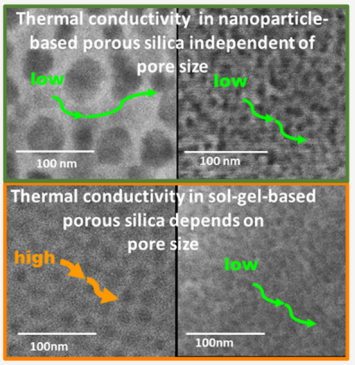

Thermal transport at the nanoscale has been an area of intense research due to various applications of nanostructured materials including thermoelectrics,[1,2] thermally insulating materials,[3,4] and thermal interface materials.[5] Nanostructuring offers unprecedented opportunities for controlling thermal transport by tuning various structural parameters.[6] Many structural factors such as pore size, total porosity, surface or interface structure, defect density, and impurities[7−10] can significantly influence the thermal conductivity of nanoscale materials. In particular, porous materials can be used as a platform for studying size effects due to their tunable syntheses and high surface area.[11] Although the size effect in crystalline materials is quite well understood,[12−14] the size effect on the thermal conductivity of amorphous materials remains underdeveloped.

Porous silica, which is based on an amorphous silica network, has received significant attention, since its high porosity can result in large reductions in thermal conductivity[11,15−17] For instance, aerogels, composed of chains of silica nanoparticles, feature extremely low thermal conductivities (0.013 W/m K) and have been used for thermal insulation in a variety of applications.[18−24] Several studies[17,25] have shown that the thermal conductivity of dense silica thin films is independent of film thickness when the thickness is greater than 100 nm, suggesting that any propagating modes contributing to the thermal conductivity have mean free paths (MFPs) below 100 nm.[12] In addition, the effective thermal conductivity of mesoporous silica at room temperature has been shown to decrease rapidly with increasing porosity.[16,26,27] Hu et al.[28] proposed phenomenological, ad hoc two-phase mixture models that described the dependence of thermal conductivity on porosity.

Notably, the effect of pore size on the thermal conductivity of nanoporous silica remains unclear. In theory, the intensity of scattering would depend on the size of the solid backbone. While pore size and wall thickness are not rigorously linked, they are generally correlated in most solution-derived porous materials. As such, with a porous structure, the MFP should be reduced when it is comparable to the pore size.[29] Some experimental studies, however, have suggested that the thermal conductivity of mesoporous silica was independent of pore size.[26,30] However, these studies only focused on silica aerogel or sol−gel networks and sampled a limited range of pore sizes. Jain et al. showed that the thermal conductivity of xerogel films depended on the pore size distribution, with micropores contributing the most to phonon scattering.[29] However, due to the different preparation processes, these samples may have different amounts of cracks, defects, and impurities that also contribute to phonon scattering, making the comparison challenging. In our previous work,[31] we suspected a dependence of thermal conductivity on pore size in mesoporous silica; however, the evidence was not strong enough to warrant a conclusion. Thus, the investigation should be extended to a

Received: February 11, 2020
Accepted: April 17, 2020
Published: April 17, 2020

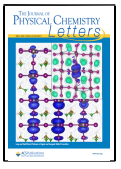

https://dx.doi.org/10.1021/acs.jpclett.0c00464
J. Phys. Chem. Lett. 2020, 11, 3731−3737

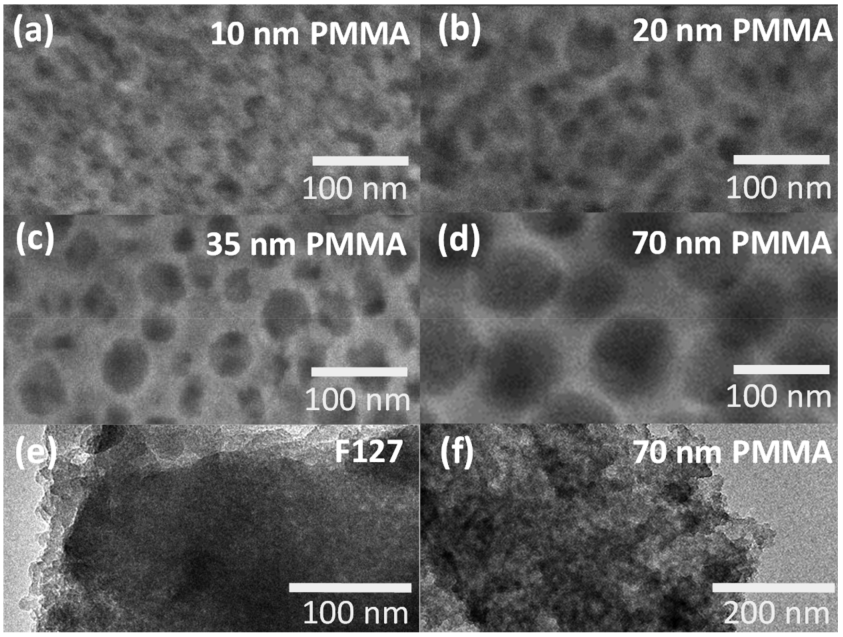

Figure 1. SEM (a–d) and transmission electron microscopy (TEM) (e,f) images of NP-based mesoporous silica films templated with PMMA colloids or Pluronic F127 with average sizes of (a) 10, (b) 20, (c) 35, (d,f) 70, and (e) 10–16 nm.

broader pore size range to gain better insight into the effect of pore size on the thermal conductivity of mesoporous silica.

The present study discusses the effect of pore size on the effective thermal conductivity of mesoporous silica films with a wide range of pore sizes and two different silica frameworks, i.e., a continuous matrix synthesized using sol–gel methods or a discontinuous network made from discrete nanoparticles. A number of sol–gel (SG)- and nanoparticle (NP)-based mesoporous silica thin films with different pore sizes were synthesized under the same conditions to reduce the effect of impurities and defects. The effective thermal conductivity in the out-of-plane direction was measured with time domain thermoreflectance (TDTR)[32,33] in vacuum at room temperature to eliminate the contribution of the gas phase on thermal transport. During thermal treatment, these films shrink in an anisotropic manner, with a greater degree of shrinkage in the out-of-plane direction compared to the in-plane direction. As such, we are measuring the upper limit of the thermal conductivity, since the porosity in the out-of-plane direction may be lower than in the in-plane direction.

Multiple NP-based mesoporous silica films with pore diameters in the range of 10–70 nm were synthesized using PMMA colloids or Pluronic triblock copolymers as the template to thoroughly examine the effect of pore size on the thermal conductivity. Figure 1a–d shows scanning electron microscopy (SEM) images of porous silica films templated with different sizes of PMMA. The average pore size estimated from the SEM images matched the average size of PMMA colloids used for the synthesis, with wide pore size distributions due to the polydisperisity of the PMMA colloids. In addition, the increase in the wall thickness of the NP-based films with increasing average pore size can be directly observed.

Figure 1e,f shows TEM images of typical F127-templated and 70 nm PMMA-templated NP-based mesoporous silica films. Since the samples were obtained from thick films, the pores are not easily visualized in transmission unless the sample is viewed directly down a pore axis, which is improbable for these disordered porous networks. Instead, one sees only differences in contrast in the films due to the absence of nanoparticles in some regions, which indicates the presence of pores somewhere within the thickness of the sample. While the pores are not easy to see, the nanoparticle building blocks are easier to observe. Figure S1 shows an image with both the pores and nanoparticle building blocks outlined for clarity. Because the nanoparticles used for all films were the same size, an increase in the thickness of the walls simply requires more nanoparticles stacked together.

The porosity and pore size distributions of NP-based mesoporous silica films templated with Pluronic F127 were analyzed by ellipsometric porosimetry at ambient temperature using toluene as the adsorbate.[34] The NP-based silica films templated with PMMA colloids could not be measured using ellipsometric porosimetry due to their large pores that scatter the light used in the ellipsometric measurement. As a result, the porosity and the pore size were measured using N_2 adsorption porosimetry on the NP-based mesoporous silica powders templated with PMMA colloids that were prepared in the same conditions as their corresponding films. Figure 2 shows the adsorption–desorption isotherms and pore size distributions for representative NP-based mesoporous silica films templated with Pluronic F127 and PMMA colloids. Both isotherms were of type IV(a) with an H2(b) hysteresis loop according to the IUPAC classification,[35,36] which indicates mesopores connected by narrow necks. The slope of the adsorption isotherm as a function of relative pressure was much steeper in the F127-templated sample (Figure 2a) than in the PMMA-templated sample (Figure 2b), suggesting a narrower pore size distribution.[37] The difference in the degree of polydispersity was also observed in the pore size distribution (Figure 2c,d). In fact, the PMMA-templated films had a bimodal pore size distribution, indicated by the two different hysteresis regions at P/P_0 = 0.45–0.75 for small pores and at P/P_0 = 0.9–1 for larger pores (Figure 2b). The small pores corresponded to the intrinsic gaps between the silica nanoparticles and ranged from 4 to 6 nm in diameter. The

https://dx.doi.org/10.1021/acs.jpclett.0c00464
J. Phys. Chem. Lett. 2020, 11, 3731–3737

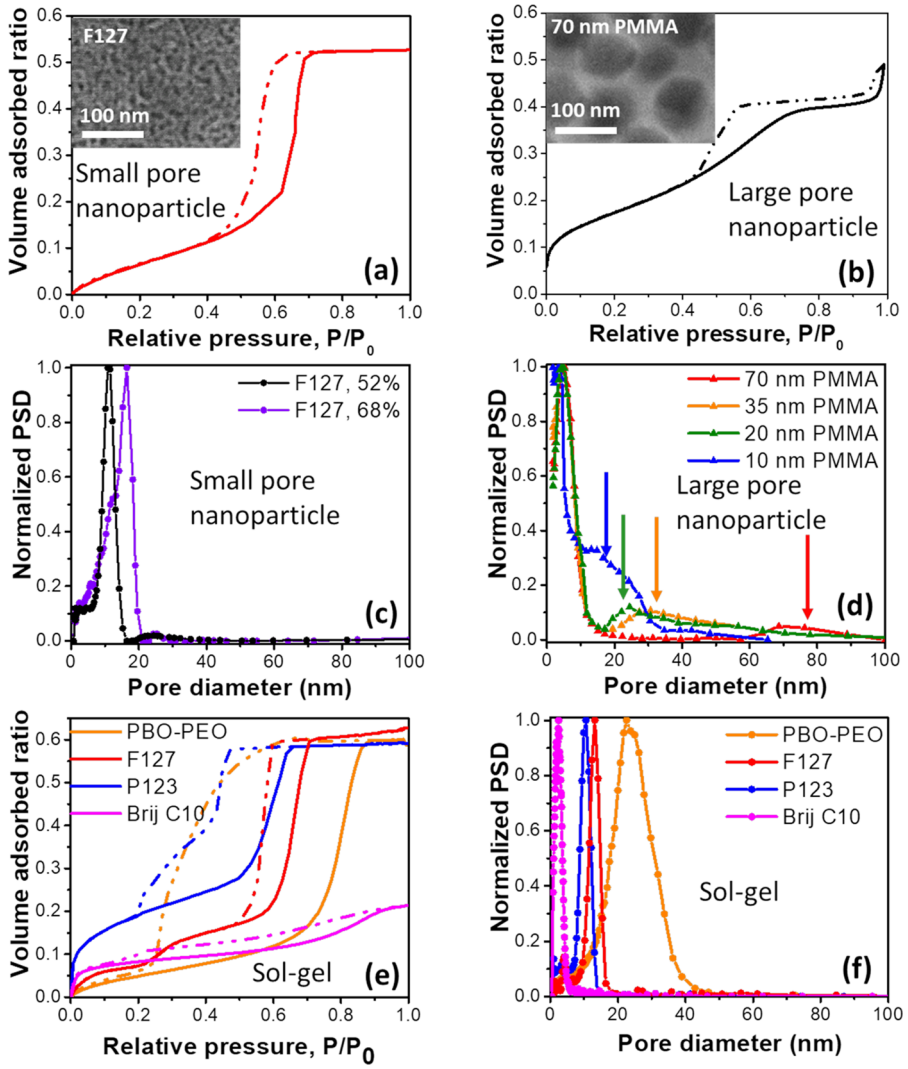

Figure 2. Isotherms and pore size distributions for NP- and SG-based mesoporous silica films templated with various polymers and surfactants. (a) Toluene adsorption/desorption isotherms for an F127-templated NP-based mesoporous silica film with a porosity of 52.5%. (b) Nitrogen adsorption/desorption isotherms for 70 nm PMMA-templated NP-based mesoporous silica with a porosity of 49%. (c) Number-weighted pore size distributions (PSDs) for F127-templated NP-based mesoporous silica films with the porosities indicated. (d) Number-weighted PSD for NP-based mesoporous silica materials with different PMMA templates. The pores between 2 and 4 nm are derived from the intrinsic gaps between the nanoparticle, while those indicated by the colored arrows are derived from the removal of the PMMA template. (e) Representative toluene adsorption/desorption isotherms for SG-based mesoporous silica films synthesized with different templates. (f) Representative number-weighted PSDs for SG-based mesoporous silica films with different templates. Insets in (a) and (b) are representative SEM images of NP-based mesoporous silica films templated with F127 and 70 nm PMMA, respectively. The pore diameters from porosimetry matched those observed in SEM images.

Table 1. Structural Characterization and Thermal Conductivity of F127- and PMMA-Templated NP-Based Mesoporous Silica Films[a]

template	porosity (%)	average interparticle pore diameter (nm)	average templated pore diameter (nm)	measured wall thickness (nm)	thermal conductivity (W/mK)
10 nm PMMA	65 ± 1	3 ± 2	10 ± 10	14 ± 4	0.096 ± 0.006
F127	68 ± 1	-	16 ± 2	7 ± 1	0.107 ± 0.005
35 nm PMMA	71 ± 1	4 ± 3	30 ± 10	25 ± 6	0.098 ± 0.005
F127	53 ± 1	-	11 ± 2	7 ± 1	0.19 ± 0.01
10 nm PMMA	49 ± 1	3 ± 2	10 ± 10	14 ± 1	0.24 ± 0.01
20 nm PMMA	50 ± 1	5 ± 3	27 ± 7	15 ± 5	0.21 ± 0.02
70 nm PMMA	49 ± 1	5 ± 3	74 ± 9	38 ± 15	0.19 ± 0.01

[a]Average pore diameters from the gaps between particles and voids from template removal are included.

large pores corresponded to the voids left after removing the PMMA template, and their size ranged from 15 to 68 nm, depending on the size of the PMMA colloids used. By contrast, the pore size distribution of NP-based mesoporous silica films templated with Pluronic F127 showed only one peak. This can be attributed to the fact that the size distributions of the

https://dx.doi.org/10.1021/acs.jpclett.0c00464
J. Phys. Chem. Lett. 2020, 11, 3731−3737

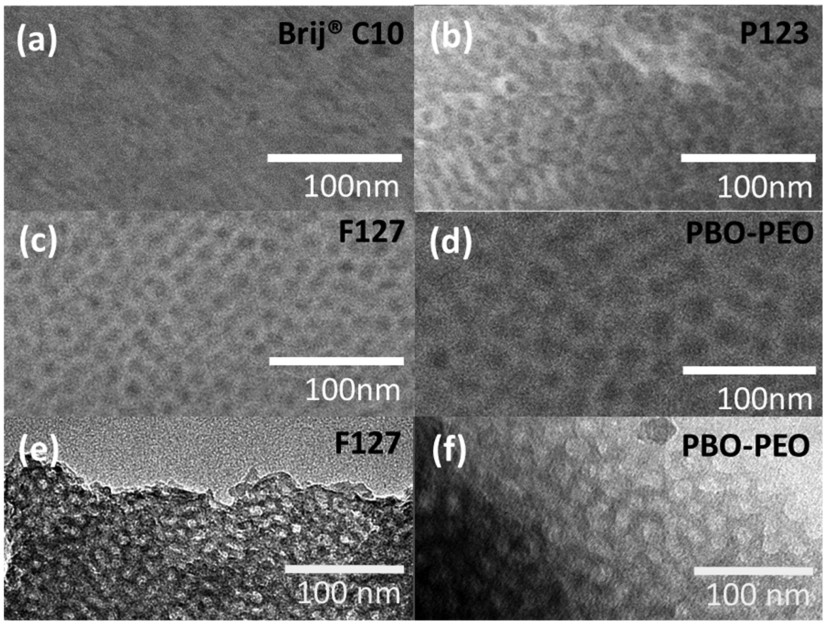

Figure 3. SEM (a–d) and TEM images (e,f) of SG-based mesoporous silica films templated by (a) BrijC10, (b) Pluronic P123, (c,e) Pluronic F127, and (d,f) PBO–PEO block copolymer. Films had increasing pore size from (a) to (d).

interparticle porosity and of the template-derived porosity were similar and overlapped.

Table 1 summarizes the structural characterization and thermal conductivity of two groups of NP-based mesoporous silica films with similar porosities but different pore diameters. The two different pore diameter values for PMMA-templated materials correspond to the intrinsic gaps between the silica nanoparticles and the voids left after removing the PMMA template, respectively. The first group had a porosity of 65–71% and pore diameter of 15–28 nm, while the second group had a porosity of 49–53% and pore diameter of 10–68 nm. The thickness of the pore walls was estimated from the SEM images. Table 1 indicates that NP-based mesoporous silica films with similar porosities had similar effective thermal conductivities despite having very different average pore sizes and, as a result, different wall thicknesses. We hypothesize that this observation is due to the fact that the thermal transport in NP-based films was determined by the heat carrier scattering between particles as well as at the boundary of each nanoparticle, both of which depend on the nanoparticle size rather than on the wall thickness.

To examine the effect of pore size on the thermal conductivity of sol–gel mesoporous silica films (SG-based mesoporous silica), multiple SG-based mesoporous silica films with pore diameters in the range of 3–23 nm were synthesized using different organic templates. Here, PMMA colloids could not be used as templates, as they are incompatible with the solvents used for sol–gel synthesis (the PMMA colloids aggregate and precipitate in ethanol). Figure 3 shows typical SEM images of the SG-based mesoporous silica films synthesized with these different templates. Those templated with CTAB and BrijC10 had very small pores between 1 and 4 nm in diameter. On the other hand, the films templated with different sized PBO–PEO block copolymers had large pores with diameters between 15 and 25 nm (Figure 3d). The block-copolymer-templated films displayed fairly ordered porous structures, as shown in Figure 3b–d. This was further supported by two-dimensional grazing-incidence small-angle X-ray scattering (2D-GISAXS) patterns, which are shown in Figure S2. The diffraction arc indicates that the pores are at least partly ordered. The intensity around the arc is not fully uniform, however, because there are only a finite number of repeat distances in the out-of-plane direction, while there is effectively an infinite number in the in-plane direction. Moreover, the in- and out-of-plane lattice spacings are also not the same, because more shrinkage occurs in the direction normal to the substrate, compared to in-plane. The result is a continuous distribution with broader peaks occurring at a higher q in the out-of-plane direction and narrower peaks occurring at a lower q in the in-plane direction. To rapidly quantify this distribution, here we report only the in-plane peak positions from Figure S2c, but all orientations are present. As expected, the inter-repeat distance, d, calculated as $d = 2\pi/q$, increases as the template size increased. Finally, TEM images (Figure 3e,f) show clear pores, which again arise because the ordered porosity allows transmission images to be collected in which all the pores line up on top of each to make clear regions of dark and light contrast.

The porosity and pore size of SG-based mesoporous silica films were measured by ellipsometric porosimetry using toluene as the adsorbate. Figure 2e,f shows toluene adsorption–desorption isotherms and pore size distributions for representative SG-based mesoporous silica films templated with BrijC10, Pluronic P123, Pluronic F127, and PBO–PEO. Here also, the hysteresis loops in the isotherms indicated the presence of mesopores connected by narrow necks. Most of the samples had a fairly narrow pore size distribution. The pore sizes from the ellipsometric porosimetry measurement were in agreement with estimates from SEM images. The pore walls' thickness w of SG-based mesoporous silica films was calculated by combining the pore radius r from ellipsometric porosimetry with the interplane spacing d from 2D-GISAXS using the equation[38]

$$w = 2\left(\frac{d}{\sqrt{3}} - r\right) \quad (1)$$

https://dx.doi.org/10.1021/acs.jpclett.0c00464
J. Phys. Chem. Lett. 2020, 11, 3731–3737

Table 2. Structural Characterization and Thermal Conductivity of SG-Based Mesoporous Silica Films Synthesized with Different Templates

template	porosity (%)	pore diameter (nm)	unit cell repeating distance (nm)	wall thickness (nm)[a]	thermal conductivity in vacuum (W/mK)
P123	59 ± 1	10 ± 1	13 ± 1	5 ± 1	0.081 ± 0.006
F127	62 ± 1	13 ± 1	14 ± 1	3 ± 1	0.096 ± 0.009
PBO−PEO	60 ± 1	24 ± 5	35 ± 3	16 ± 6	0.21 ± 0.01
P123	43 ± 1	6 ± 1	11 ± 5	7 ± 5	0.157 ± 0.008
F127	44 ± 1	8 ± 2	14 ± 1	8 ± 2	0.24 ± 0.01
PBO−PEO	44 ± 1	14 ± 7	23 ± 1	13 ± 7	0.29 ± 0.02
CTAB	16 ± 2	2 ± 1	N/A	2 ± 1	0.31 ± 0.02
BrijC10	21 ± 2	2 ± 1	N/A	2 ± 1	0.28 ± 0.02
P123	18 ± 2	3 ± 1	N/A	4 ± 1	0.40 ± 0.02
F127	19 ± 2	4 ± 1	N/A	5 ± 2	0.41 ± 0.02

[a]Wall thickness calculated from GISAXS and porosimetry data. For samples without GISAXS data, a range was estimated from SEM images.

In general, sol−gel silica films made with larger templates also displayed thicker walls. For films that lacked periodicity (at a low m_{poly}/m_{SiO_2} ratio or templated by CTAB and BrijC10), a range of wall thicknesses were measured and estimated from SEM images.

To isolate the effect of wall thickness from porosity on the thermal conductivity, Table 2 and Figure 4 summarize the characterization of three groups of SG-based mesoporous silica films with similar porosities but different pore diameters and wall thicknesses. The first group had a porosity of 59−62% and pore diameter ranging from 10 to 23 nm, the second group had a porosity of 43−45% and pore diameter ranging from 5 to 15 nm, while the third group had a porosity of 18−22% and pore diameter ranging from 2 to 4 nm. Table 2 indicates that SG-based mesoporous silica films with a similar porosity but larger pore size had larger effective thermal conductivity. For a given porosity, the SG-based mesoporous silica films templated with CTAB and BrijC10 had lower thermal conductivity than films templated with Pluronic P123 templates, followed by films templated with Pluronic F127 and then PBO−PEO. This order correlated with the pore sizes created by these templates in SG-based mesoporous silica films.

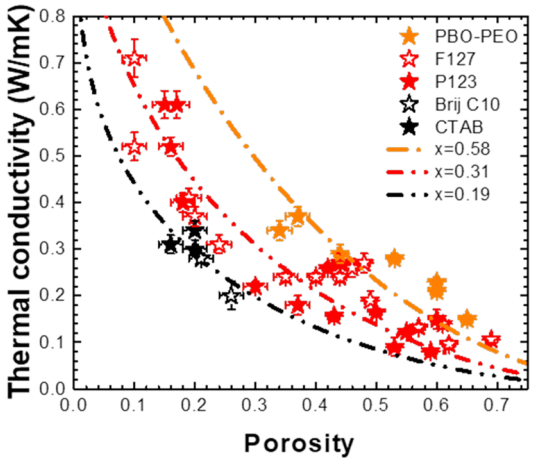

Figure 4. Thermal conductivity as a function of porosity for SG-based mesoporous silica films templated using different polymer templates to provide a range of pore diameters (BrijC10 and CTAB from 2 to 4 nm, F127 and P123 from 5 to 15 nm, PBO−PEO from 15 to 25 nm), measured under vacuum. Dashed lines correspond to fits to the PWSM model with fit values shown in the legend.

Such a positive correlation between pore size and thermal conductivity at a fixed porosity had been previously observed in porous crystals.[39−41] In crystals, the heat is carried by traveling phonons with a certain distribution of phonon MFPs. The scattering of phonons at the boundary between pores and the solid phase can reduce the effective phonon MFPs and thus the thermal conductivity. Thus, the intrinsic mean free path determines the maximum pore size that would affect the thermal conductivity. For example, in silicon, the suppression of phonon MFPs can be significant when the pore size is about 1 μm, because the intrinsic MFPs of a substantial portion of phonons can exceed 1 μm.[14] Analogous to silicon, the correlation between pore size and thermal conductivity in amorphous SG-based mesoporous silica films can also be attributed to the vibrational modes scattering near the pores. Importantly, it indicates that the MFPs for a non-negligible fraction of the vibrational modes are between 1 to 10 nm. This result is also consistent with the recent molecular dynamic simulation results and experimental results from ballistic transport across $Si/SiO_2/Si$ nanostructures.[17,42]

A porosity weighted simple medium (PWSM) model has been proposed to account for the combined effect of pore size and shape and thermal contact between particles by using a fitting parameter x.[26,43] The parameter x can vary between 0 and infinity, corresponding to the serial and parallel effective medium approximations, respectively. This model has been used extensively for various porous materials including silica xerogels[28] and templated mesoporous silica.[26,44] Considering that the disperse phase in the pores of our sol−gel mesoporous silica films is vacuum, the PWSM model simplifies to[26]

$$\kappa_{eff} = \kappa_{SiO_2}(1 - \phi_p)(1 - \phi_p^x) \quad (2)$$

Fitting the PWSM model to our experimental data yielded x = 0.19, 0.31, and 0.58 for small (CTAB and BrijC10), medium (P123 and F127), and large (PBO−PEO) pore sizes, respectively. Figure 4 plots the effective thermal conductivities of sol−gel-based mesoporous silica films as a function of porosity and compares them with the three predictions obtained from eq 2. A value of x approaching 0 corresponds to the asymptotic case captured by the serial model, which can be physically represented as a lamellar structure consisting of a series of silica layers separated by layers of air, all aligned with the layers perpendicular to the direction of heat flow; this results in the lowest thermal conductivity possible for a given porosity. We find that x increases as the pore size and corresponding wall thickness increase, suggesting that thicker walls enhanced the through-plane heat conduction captured in

https://dx.doi.org/10.1021/acs.jpclett.0c00464
J. Phys. Chem. Lett. 2020, 11, 3731−3737

the limiting case by the parallel model (which physically corresponds to the same alternating air and silica layers, this time with the layers oriented parallel to the direction of heat flow). In an attempt to more explicitly capture the effect of pore size on the thermal conductivity of our material, Figure S3 further shows the same data fit with a model developed by Alvarez et al. that contains explicit pore size dependence.[45] While the fit parameters are reasonable, the fit quality is relatively poor, likely because the model was developed for crystalline porous materials.

Overall, in this work, we examined how wall thickness controls thermal conductivity for mesoporous silica materials with different pore sizes and corresponding wall thicknesses that are made from different building blocks. We find a fundamental difference in how wall thickness effects thermal conductivity in SG-based versus NP-based mesoporous silica films. As revealed by the TEM images in Figure 1e,f, the walls of the NP-based film are made of discrete interconnected silica nanoparticles, which suggests that the characteristic length limiting the vibrational MFP is the size of the silica nanoparticles, not the thickness of the walls. As such, changing the pore size, and ultimately the wall thickness, should not significantly affect effective thermal conductivity. By contrast, SG-based mesoporous silica is composed of a continuous network surrounding mesopores. Here, the characteristic length limiting the vibrational MPF is the thickness of the pore walls. Because SG-based mesoporous silica with a large pore size also tends to have large wall thickness, heat carriers traveling in SG-based mesoporous silica with large pores will experience less scattering, resulting in higher effective thermal conductivity.

This work thus helps expand our understanding of heat transfer at the nanoscale and opens new avenues for tailoring the thermal conductivity of nanostructured materials by means other than porosity or composition. These results also help to explain some of the seemingly contradictory data in the literature. Depending on the exact synthesis conditions, nontemplated sol−gel materials can be composed of more continuous, filamentous materials or more aggregated nanoparticles.[27] With our new understanding, it would be expected that thermal conductivity in some systems would depend strongly on wall thickness, while in others, it would not.

EXPERIMENTAL METHODS

Sol−gel- and nanoparticle-based mesoporous silica thin films were prepared by evaporation-induced self-assembly according to previously reported methods.[31] Detailed procedures of the synthesis and characterization of the films are provided in the Supporting Information.

ASSOCIATED CONTENT

Supporting Information

The Supporting Information is available free of charge at https://pubs.acs.org/doi/10.1021/acs.jpclett.0c00464.

Details of synthesis, structural characterization, and thermal conductivity measurement; TEM images for nanoparticle-based films; 2D-GISAXS data for SG-based mesoporous silica films; thermal conductivity vs porosity curves for sol−gel-based samples fit using an alternative model (PDF)

AUTHOR INFORMATION

Corresponding Author

Sarah H. Tolbert − *Department of Chemistry and Biochemistry and Department of Materials Science and Engineering, UCLA, Los Angeles, California 90095-1569, United States;* orcid.org/0000-0001-9969-1582; Email: tolbert@chem.ucla.edu

Authors

Yan Yan − *Department of Chemistry and Biochemistry, UCLA, Los Angeles, California 90095-1569, United States*

Man Li − *Department of Mechanical Engineering, UCLA, Los Angeles, California 90095, United States*

Sophia King − *Department of Chemistry and Biochemistry, UCLA, Los Angeles, California 90095-1569, United States*

Tiphaine Galy − *Department of Mechanical Engineering, UCLA, Los Angeles, California 90095, United States*

Michal Marszewski − *Department of Mechanical Engineering, UCLA, Los Angeles, California 90095, United States;* orcid.org/0000-0002-4157-3046

Joon Sang Kang − *Department of Mechanical Engineering, UCLA, Los Angeles, California 90095, United States*

Laurent Pilon − *Department of Mechanical Engineering, UCLA, Los Angeles, California 90095, United States;* orcid.org/0000-0001-9459-8207

Yongjie Hu − *Department of Mechanical Engineering, UCLA, Los Angeles, California 90095, United States;* orcid.org/0000-0001-7225-1130

Complete contact information is available at: https://pubs.acs.org/10.1021/acs.jpclett.0c00464

Notes

The authors declare no competing financial interest.

ACKNOWLEDGMENTS

This work was supported by the U.S. Department of Energy (DOE), Advanced Research Projects Agency-Energy (ARPA-E) under Award Number DE-AR0000738. Y.Y. is grateful to the Chinese Scholar Council for financial support in the form of a graduate fellowship. The authors acknowledge the use of instruments at the Electron Imaging Center for NanoMachines supported by NIH (1S10RR23057) and the California NanoSystems Institute (CNSI) at UCLA. This manuscript contains X-ray data that were collected at the Stanford Synchrotron Radiation Lightsource. Use of the Stanford Synchrotron Radiation Lightsource, SLAC National Accelerator Laboratory, is supported by the U.S. Department of Energy, Office of Science, Office of Basic Energy Sciences, under Contract DE-AC02-76SF00515.

REFERENCES

(1) Boukai, A. I.; Bunimovich, Y.; Tahir-Kheli, J.; Yu, J.-K.; Goddard, W. A., III; Heath, J. R. Silicon Nanowires as Efficient Thermoelectric Materials. *Nature* **2008**, *451* (7175), 168−171.

(2) Dresselhaus, M. S.; Chen, G.; Tang, M. Y.; Yang, R. G.; Lee, H.; Wang, D. Z.; Ren, Z. F.; Fleurial, J.; Gogna, P. New Directions for Low-Dimensional Thermoelectric Materials. *Adv. Mater.* **2007**, *19* (8), 1043−1053.

(3) Costescu, R. M. Ultra-Low Thermal Conductivity in W/Al_2O_3 Nanolaminates. *Science* **2004**, *303* (5660), 989−990.

(4) Hrubesh, L. W.; Pekala, R. W. Thermal Properties of Organic and Inorganic Aerogels. *J. Mater. Res.* **1994**, *9* (03), 731−738.

(5) Prasher, R. Thermal Interface Materials: Historical Perspective, Status, and Future Directions. *Proc. IEEE* **2006**, *94* (8), 1571−1586.
(6) Cahill, D. G.; Ford, W. K.; Goodson, K. E.; Mahan, G. D.; Majumdar, A.; Maris, H. J.; Merlin, R.; Phillpot, S. R. Nanoscale Thermal Transport. *J. Appl. Phys.* **2003**, *93* (2), 793−818.
(7) Sansoz, F. Surface Faceting Dependence of Thermal Transport in Silicon Nanowires. *Nano Lett.* **2011**, *11* (12), 5378−5382.
(8) Gu, H.; Wang, H. Effect of Strain on Thermal Conductivity of Amorphous Silicon Dioxide Thin Films: A Molecular Dynamics Study. *Comput. Mater. Sci.* **2018**, *144*, 133−138.
(9) Alam, M. T.; Raghu, A. P.; Haque, M. A.; Muratore, C.; Voevodin, A. A. Structural Size and Temperature Dependence of Solid to Air Heat Transfer. *Int. J. Therm. Sci.* **2013**, *73*, 1−7.
(10) Tian, Z.; Hu, H.; Sun, Y. A Molecular Dynamics Study of Effective Thermal Conductivity in Nanocomposites. *Int. J. Heat Mass Transfer* **2013**, *61* (1), 577−582.
(11) Hopkins, P. E.; Rakich, P. T.; Olsson, R. H.; El-Kady, I. F.; Phinney, L. M. Origin of Reduction in Phonon Thermal Conductivity of Microporous Solids. *Appl. Phys. Lett.* **2009**, *95* (16), 161902.
(12) Marconnet, A. M.; Asheghi, M.; Goodson, K. E. From the Casimir Limit to Phononic Crystals: 20 Years of Phonon Transport Studies Using Silicon-on-Insulator Technology. *J. Heat Transfer* **2013**, *135* (6), 061601.
(13) Zhang, H.; Hua, C.; Ding, D.; Minnich, A. J. Length Dependent Thermal Conductivity Measurements Yield Phonon Mean Free Path Spectra in Nanostructures. *Sci. Rep.* **2015**, *5* (1), 9121.
(14) Hu, Y.; Zeng, L.; Minnich, A. J.; Dresselhaus, M. S.; Chen, G. Spectral Mapping of Thermal Conductivity through Nanoscale Ballistic Transport. *Nat. Nanotechnol.* **2015**, *10* (8), 701−706.
(15) Deng, Z.; Wang, J.; Wu, A.; Shen, J.; Zhou, B. High Strength SiO2 Aerogel Insulation. *J. Non-Cryst. Solids* **1998**, *225*, 101−104.
(16) Hopkins, P. E.; Kaehr, B.; Phinney, L. M.; Koehler, T. P.; Grillet, A. M.; Dunphy, D.; Garcia, F.; Brinker, C. J. Measuring the Thermal Conductivity of Porous, Transparent SiO2 Films With Time Domain Thermoreflectance. *J. Heat Transfer* **2011**, *133* (6), 061601.
(17) Larkin, J. M.; McGaughey, A. J. H. Thermal Conductivity Accumulation in Amorphous Silica and Amorphous Silicon. *Phys. Rev. B: Condens. Matter Mater. Phys.* **2014**, *89* (14), 1−12.
(18) Schmidt, M.; Schwertfeger, F. Applications for Silica Aerogel Products. *J. Non-Cryst. Solids* **1998**, *225*, 364−368.
(19) Reim, M.; Reichenauer, G.; Körner, W.; Manara, J.; Arduini-Schuster, M.; Korder, S.; Beck, A.; Fricke, J. Silica-Aerogel Granulate − Structural, Optical and Thermal Properties. *J. Non-Cryst. Solids* **2004**, *350*, 358−363.
(20) Reim, M.; Körner, W.; Manara, J.; Korder, S.; Arduini-Schuster, M.; Ebert, H.-P.; Fricke, J. Silica Aerogel Granulate Material for Thermal Insulation and Daylighting. *Sol. Energy* **2005**, *79* (2), 131−139.
(21) Baetens, R.; Jelle, B. P.; Gustavsen, A. Aerogel Insulation for Building Applications: A State-of-the-Art Review. *Energy Build* **2011**, *43* (4), 761−769.
(22) Chen, K.; Neugebauer, A.; Goutierre, T.; Tang, A.; Glicksman, L.; Gibson, L. J. Mechanical and Thermal Performance of Aerogel-Filled Sandwich Panels for Building Insulation. *Energy Build* **2014**, *76*, 336−346.
(23) Venkateswara Rao, A.; Pajonk, G. M.; Haranath, D. Synthesis of Hydrophobic Aerogels for Transparent Window Insulation Applications. *Mater. Sci. Technol.* **2001**, *17* (3), 343−348.
(24) Wei, T.; Chang, T.-F.; Lu, S.; Chang, Y. Preparation of Monolithic Silica Aerogel of Low Thermal Conductivity by Ambient Pressure Drying. *J. Am. Ceram. Soc.* **2007**, *90* (7), 2003−2007.
(25) Shenogin, S.; Bodapati, A.; Keblinski, P.; McGaughey, A. J. H. Predicting the Thermal Conductivity of Inorganic and Polymeric Glasses: The Role of Anharmonicity. *J. Appl. Phys.* **2009**, *105* (3), 034906.
(26) Coquil, T.; Richman, E. K.; Hutchinson, N. J.; Tolbert, S. H.; Pilon, L. Thermal Conductivity of Cubic and Hexagonal Mesoporous Silica Thin Films. *J. Appl. Phys.* **2009**, *106* (3), 034910.
(27) Lu, X.; Caps, R.; Fricke, J.; Alviso, C. T.; Pekala, R. W. Correlation between Structure and Thermal Conductivity of Organic Aerogels. *J. Non-Cryst. Solids* **1995**, *188* (3), 226−234.
(28) Hu, C.; Morgen, M.; Ho, P. S.; Jain, A.; Gill, W. N.; Plawsky, J. L.; Wayner, P. C. Thermal Conductivity Study of Porous Low- *k* Dielectric Materials. *Appl. Phys. Lett.* **2000**, *77* (1), 145−147.
(29) Jain, A.; Rogojevic, S.; Ponoth, S.; Gill, W. N.; Plawsky, J. L.; Simonyi, E.; Chen, S.-T.; Ho, P. S. Processing Dependent Thermal Conductivity of Nanoporous Silica Xerogel Films. *J. Appl. Phys.* **2002**, *91* (5), 3275−3281.
(30) Liu, J.; Gan, D.; Hu, C.; Kiene, M.; Ho, P. S.; Volksen, W.; Miller, R. D. Porosity Effect on the Dielectric Constant and Thermomechanical Properties of Organosilicate Films. *Appl. Phys. Lett.* **2002**, *81* (22), 4180−4182.
(31) Yan, Y.; King, S. C.; Li, M.; Galy, T.; Marszewski, M.; Kang, J. S.; Pilon, L.; Hu, Y.; Tolbert, S. H. Exploring the Effect of Porous Structure on Thermal Conductivity in Templated Mesoporous Silica Films. *J. Phys. Chem. C* **2019**, *123* (35), 21721−21730.
(32) Li, M.; Kang, J. S.; Hu, Y. Anisotropic Thermal Conductivity Measurement Using a New Asymmetric-Beam Time-Domain Thermoreflectance (AB-TDTR) Method. *Rev. Sci. Instrum.* **2018**, *89* (8), 084901.
(33) Kang, J. S.; Li, M.; Wu, H.; Nguyen, H.; Hu, Y. Experimental Observation of High Thermal Conductivity in Boron Arsenide. *Science* **2018**, *361* (6402), 575−578.
(34) Baklanov, M. R.; Mogilnikov, K. P.; Polovinkin, V. G.; Dultsev, F. N. Determination of Pore Size Distribution in Thin Films by Ellipsometric Porosimetry. *J. Vac. Sci. Technol., B: Microelectron. Process. Phenom.* **2000**, *18* (3), 1385−1391.
(35) Gregg, S. J.; Sing, K. S. W. *Adsorption, Surface Area and Porosity*, Second ed; Academic Press Inc., Ltd: London, 1982.
(36) Thommes, M.; Kaneko, K.; Neimark, A. V.; Olivier, J. P.; Rodriguez-Reinoso, F.; Rouquerol, J.; Sing, K. S. W. Physisorption of Gases, with Special Reference to the Evaluation of Surface Area and Pore Size Distribution (IUPAC Technical Report). *Pure Appl. Chem.* **2015**, *87* (9−10), 1051−1069.
(37) Kruk, M.; Jaroniec, M.; Ko, C. H.; Ryoo, R. Characterization of the Porous Structure of SBA-15. *Chem. Mater.* **2000**, *12* (7), 1961−1968.
(38) Smarsly, B.; Gibaud, A.; Ruland, W.; Sturmayr, D.; Brinker, C. J. Quantitative SAXS Analysis of Oriented 2D Hexagonal Cylindrical Silica Mesostructures in Thin Films Obtained from Nonionic Surfactants. *Langmuir* **2005**, *21* (9), 3858−3866.
(39) Song, D.; Chen, G. Thermal Conductivity of Periodic Microporous Silicon Films. *Appl. Phys. Lett.* **2004**, *84* (5), 687−689.
(40) Tang, J.; Wang, H. T.; Lee, D. H.; Fardy, M.; Huo, Z.; Russell, T. P.; Yang, P. Holey Silicon as an Efficient Thermoelectric Material. *Nano Lett.* **2010**, *10* (10), 4279−4283.
(41) Seol, J. H.; Barth, D. S.; Zhu, J.; Ćoso, D.; Hippalgaonkar, K.; Lim, J.; Han, J.; Zhang, X.; Majumdar, A. Tunable Thermal Conductivity in Mesoporous Silicon by Slight Porosity Change. *Appl. Phys. Lett.* **2017**, *111* (6), 063104.
(42) Yang, L.; Zhang, Q.; Cui, Z.; Gerboth, M.; Zhao, Y.; Xu, T. T.; Walker, D. G.; Li, D. Ballistic Phonon Penetration Depth in Amorphous Silicon Dioxide. *Nano Lett.* **2017**, *17* (12), 7218−7225.
(43) Fricke, J.; Lu, X.; Wang, P.; Büttner, D.; Heinemann, U. Optimization of Monolithic Silica Aerogel Insulants. *Int. J. Heat Mass Transfer* **1992**, *35* (9), 2305−2309.
(44) Zhu, W.; Zheng, G.; Cao, S.; He, H. Thermal Conductivity of Amorphous SiO2thin Film: A Molecular Dynamics Study. *Sci. Rep.* **2018**, *8* (1), 1−9.
(45) Alvarez, F. X.; Jou, D.; Sellitto, A. Pore-Size Dependence of the Thermal Conductivity of Porous Silicon: A Phonon Hydrodynamic Approach. *Appl. Phys. Lett.* **2010**, *97* (3), 033103.

https://dx.doi.org/10.1021/acs.jpclett.0c00464
J. Phys. Chem. Lett. 2020, 11, 3731−3737